

Giant interface spin-orbit torque in NiFe/Pt bilayers

Shu-Fa Li(李树发), Tao Zhu(朱涛)
Citation: Chin. Phys. B . 2020, 29(8): 087102 . **doi:** 10.1088/1674-1056/ab9292
Journal homepage: http://cpb.iphy.ac.cn; http://iopscience.iop.org/cpb

What follows is a list of articles you may be interested in

A review of current research on spin currents and spin-orbit torques

Xiao-Yu Feng(冯晓玉), Qi-Han Zhang(张琪涵), Han-Wen Zhang(张瀚文), Yi Zhang(张祎), Rui Zhong(钟瑞), Bo-Wen Lu(卢博文), Jiang-Wei Cao(曹江伟), Xiao-Long Fan(范小龙)
Chin. Phys. B . 2019, 28(10): 107105 . **doi:** 10.1088/1674-1056/ab425e

Global phase diagram of a spin-orbit-coupled Kondo lattice model on the honeycomb lattice

Xin Li(李欣), Rong Yu(俞榕), Qimiao Si
Chin. Phys. B . 2019, 28(7): 077102 . **doi:** 10.1088/1674-1056/28/7/077102

Graphene-like Be_3X_2 (X=C, Si, Ge, Sn): A new family of two-dimensional topological insulators

Lingling Song(宋玲玲), Lizhi Zhang(张礼智), Yurou Guan(官雨柔), Jianchen Lu(卢建臣), Cuixia Yan(闫翠霞), Jinming Cai(蔡金明)
Chin. Phys. B . 2019, 28(3): 037101 . **doi:** 10.1088/1674-1056/28/3/037101

Spin texturing in quantum wires with Rashba and Dresselhaus spin-orbit interactions and in-plane magnetic field

B Gisi, S Sakiroglu, İ Sokmen
Chin. Phys. B . 2016, 25(1): 017103 . **doi:** 10.1088/1674-1056/25/1/017103

Tb doping induced enhancement of anomalous Hall effect in NiFe films

Zhu Jia-Peng, Ma Li, Zhou Shi-Ming, Miao Jun, Jiang Yong
Chin. Phys. B . 2015, 24(1): 017101 . **doi:** 10.1088/1674-1056/24/1/017101

Giant interface spin-orbit torque in NiFe/Pt bilayers*

Shu-Fa Li(李树发)[1] and Tao Zhu(朱涛)[2,†]

[1] College of Electronics and Information Engineering, Guangdong Ocean University, Zhanjiang 524088, China
[2] Beijing National Laboratory for Condensed Matter Physics and Institute of Physics, Chinese Academy of Sciences, Beijing 100190, China

(Received 20 April 2020; revised manuscript received 11 May 2020; accepted manuscript online 13 May 2020)

The current-induced spin-orbit torque (SOT) plays a dominant role to manipulate the magnetization in a heavy metal/ferromagnetic metal bilayer. We separate the contributions of interfacial and bulk spin-orbit coupling (SOC) to the effective field of field-like SOT in a typical NiFe/Pt bilayer by planar Hall effect (PHE). The effective field from interfacial SOC is directly measured at the transverse PHE configuration. Then, at the longitudinal configuration, the effective field from bulk SOC is determined, which is much smaller than that from interfacial SOC. The giant interface SOT in NiFe/Pt bilayers suggests that further analysis of interfacial effects on the current-induced manipulation of magnetization is necessary.

Keywords: spin-orbit coupling, planar Hall effect, spin-orbit torques, spin Hall effect

PACS: 71.70.Ej, 72.25.Ba, 75.76.+j **DOI:** 10.1088/1674-1056/ab9292

1. Introduction

The current-induced manipulation of magnetization in a ferromagnet is currently one of the most active areas in spintronics. This control has been more efficiently realized by the current-induced spin-orbit torques (SOTs)[1–3] than the conventional spin-transfer torques,[4,5] whereby the strong spin-orbit coupling (SOC) of a heavy metal (HM) transfers the carrier momentum directly to the local magnetization of the ferromagnet (FM).[6–8] Indeed, in an FM/HM bilayer or an oxide/FM/HM heterostructure,[10–17] the spin current produced by the spin-orbit effect applies a torque on the magnetization. This torque can excite or reverse the magnetization direction, hence it is expected to be applied in the magnetic memories, logic and data-storage devices.[6–9] The current-induced SOT has been observed in Pt/Co/AlO_x, and it was attributed to the Rashba SOC due to the structural inversion symmetry breaking.[16] However, some researchers argued that the torque in this film emerges from the spin Hall effect (SHE) of the HM layer but not the Rashba effect at the interface.[18] Since then, the complex nature of the SOT in FM/HM multilayers has been demonstrated by many observations.[6,7,15,19–22] Owing to both SHE and Rashba effects playing an important role and the very similar effects of them on magnetization dynamics, it is still difficult to clearly clarify the physical origin of the SOT in FM/HM multilayer. For example, the nonlocal effect of measurement in the NiFe/Pt bilayer indicates that the effective field of SOT does not rely on the FM/HM interface,[23] but it still lack enough proof to conclude the contribution of SHE from a Pt layer dominates the mechanism of SOT in such a simple FM/HM system. Moreover, an obvious interfacial SOT in the Al_2O_3/NiFe/Ti heterostructure with a weak SOC of Ti layer was found.[22] These results suggest both interfacial and bulk spin-orbit effects in typical NiFe/Pt systems. Indeed, besides the bulk SOT from the Pt layer, the interfacial SOT was simultaneously observed in NiFe/Pt bilayer,[24] which generates from the Rashba SOC due to the structure inversion asymmetry. However, researchers demonstrated that this interfacial spin-orbit effect in NiFe/Pt bilayer arises from the interfacial SHE at the NiFe/Pt interface.[25] Therefore, separating the interfacial and bulk SOTs in an experiment becomes very crucial, which will offer further insight into the mechanism of the SOT for FM/HM multilayers.

In this paper, we develop the PHE measurement to separate the two mechanisms in a typical NiFe/Pt bilayer deposited on a SiO_2/Si substrate. Using the PHE measurement at transverse configuration, *i.e.*, the current perpendicular the external field ($I \perp H$), the interfacial spin-orbit effective field $h_{\mathrm{FL}}^{\mathrm{i}}$ is directly measured. The bulk spin-orbit effective field $h_{\mathrm{FL}}^{\mathrm{b}}$ arising from the SHE of a Pt layer is obtained by measuring the effective field at the longitudinal configuration of the PHE measurement, *i.e.*, the current parallel to the external field ($I \parallel H$), and then subtracting the effective field measured at the transverse PHE configuration. Our results demonstrate both interfacial and bulk field-like SOTs in the NiFe/Pt bilayers. The interfacial spin-orbit effective field arising from interfacial SOC between NiFe and the substrate, $h_{\mathrm{FL}}^{\mathrm{i}}$, is about 4 times larger than $h_{\mathrm{FL}}^{\mathrm{b}}$ arising from bulk Pt.

2. Sample and experimental setup

NiFe(2.2)/Pt(d) bilayers with different Pt thicknesses sputter-deposited on the SiO_2/Si substrate were patterned into a standard Hall bar with 1 mm width and 10 mm length by

*Project supported by the National Natural Science Foundation of China (Grant No. 11574375).
†Corresponding author. E-mail: tzhu@iphy.ac.cn
© 2020 Chinese Physical Society and IOP Publishing Ltd

using the photolithography, and then performed in the PHE measurement at room temperature. Notice that the numbers in brackets are nominal thicknesses in nanometers. As shown in Fig. 1(a), we define the longitudinal configuration of the PHE measurement as the experimental setup with current paralleling to the external field ($I \parallel H$), which is the conventional PHE measurement.[23] On the other hand, the PHE voltage is also measured in a transverse configuration, where I is perpendicular to H ($I \perp H$) and flows along the y-axis, as shown in Fig. 1(b). Next, we will obtain the in-plane effective fields along the y or x axis in the longitudinal or transverse configuration of the PHE measurement, hereafter named as h_y or h_x, respectively. Further details on preparation and measurement of the samples can be found in Ref. [26].

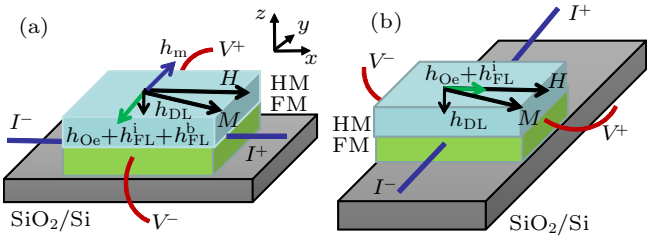


Fig. 1. Schematic diagrams of effective spin-orbit fields (a) in the longitudinal configuration ($I \parallel H$) and (b) in the transverse configuration ($I \perp H$) of PHE measurements.

3. Simulations

Figure 2 shows the simulation results of the PHE measurement for a NiFe/Pt bilayer with an in-plane magnetization. For such a film, the contribution of the current induced out-of-plane effective fields $h_{\rm DL}$ to the transverse voltage V_{xy} can be neglected.[23,26] Hence, V_{xy} mainly composes of the PHE signal and writes as[23,26]

$$V_{xy} \approx V_{\rm PHE} = \frac{I}{d}\Delta\rho \sin\phi_{\rm M}\cos\phi_{\rm M}, \tag{1}$$

where $\Delta\rho$ is the anisotropic resistivity. At the transverse configuration of PHE measurement as shown in Fig. 2(a), the in-plane magnetization direction $\phi_{\rm M}$ is determined by the competition of H, uniaxial anisotropy $K_{\rm u}$ and h_x based on the Stoner–Wohlfarth model.[27,28] In this geometry, the free energy is written as

$$\begin{aligned} E \;=\; & -M_{\rm s}H\cos(\phi_{\rm H}-\phi_{\rm M}) \\ & + K_{\rm u}\sin^2(\phi_{\rm M}-\phi_{\rm u}) - M_{\rm s}h_x\cos\phi_{\rm M}, \end{aligned} \tag{2}$$

$\phi_{\rm u}$ and $\phi_{\rm H}$ are the angles of easy axis and H apart from the x-axis, respectively. Finally, we can obtain h_x by using the equation of minimum free energy,

$$\begin{aligned} \frac{\partial E}{\partial\phi_{\rm M}} \;=\; & 2H\sin(\phi_{\rm M}-\phi_{\rm H}) \\ & + H_{\rm u}\sin[2(\phi_{\rm M}-\phi_{\rm u})] + 2h_x\sin\phi_{\rm M} = 0, \end{aligned} \tag{3}$$

where $H_{\rm u} = 2K_{\rm u}/M_{\rm s}$ is the anisotropic effective filed.

Notice that direction of the easy axis at the transverse PHE configuration is perpendicular to the one at the longitudinal configuration. Hence, the angle $\phi_{\rm u}$ is different between them. At the transverse configuration, we set $\phi_{\rm u} = 60^\circ$ in the simulations. For convenience, we actually calculate the resistance R_{xy} curve, which is expressed as $R_{xy} = V_{xy}/I$, but not the voltage curve. R_{xy} curves versus h_x were simulated with Eqs. (1) and (3). The parameters of $M_{\rm s} = 760$ emu/cm^3, $K_{\rm u} = 150$ erg/cm^3, $\phi_{\rm H} = 4^\circ$, $\Delta\rho = 0.37\ \Omega$ /nm, and $d = 3$ nm were used in the calculations. As shown in Fig. 2(b), the R_{xy} curve only induced by h_x moves along the x-axis, and the shift increases with the increase of h_x. As h_x reverses its sign, the R_{xy} curve moves to the opposite direction. This indicates that the current-induced effective field h_x can be extracted from the shift of the resistance curve measured at the transverse PHE configuration.

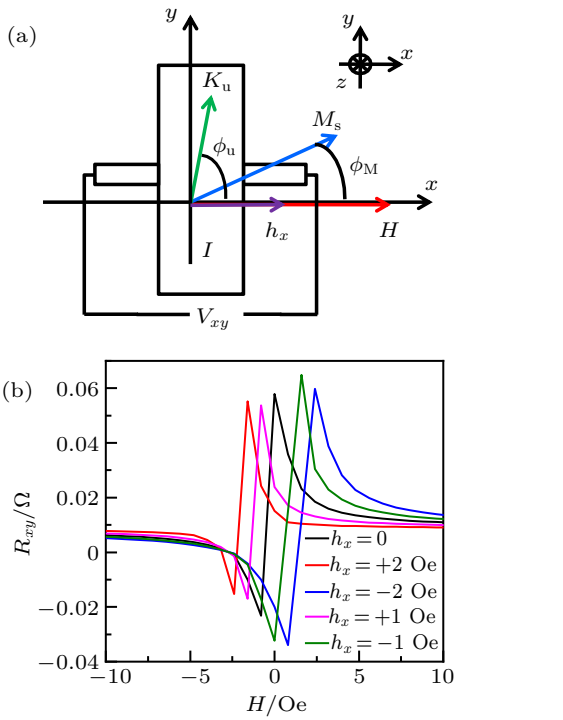


Fig. 2. (a) The schematic of NiFe/Pt bilayer at the transverse configuration of the PHE measurement. The additional field of h_x presents the effective field of the field-like SOT. (b) The field dependences of the resistance R_{xy} with various h_x. The parameters in the simulation are given in text.

4. Results and discussion

Figure 3(a) shows the representative R_{xy}–H curve of NiFe(2.2)/Pt(3) bilayer measured at the transverse configuration ($I \perp H$) of the PHE measurement. One can found that, under a quite small current $I = 0.2$ mA, the resistance curve does not move along the x-axis. However, it shifts significantly along the x-axis as the current increases to 15 mA, and it moves to the opposite direction as the current reverses its sign. According to the simulations in Fig. 2(b), the shift of the

resistance curve is due to the effective field h_x. The shift of the resistance curve from +0.2 mA to +15 mA is −0.39 Oe and the one is +0.4 Oe as the curve shifts from −0.2 mA to −15 mA, which is in agreement well with the calculated one by fitting the resistance curves with Eqs. (1) and (3). As the fitting shown in the inset of Fig. 3(a), we obtain $h_x = -0.39$ Oe or +0.41 Oe for $I = +15$ mA or −15 mA, respectively, by using the above parameters and setting $\phi_u = 55°$. Hence, we obtain $h_x = 0.395$ Oe at $I = 15$ mA. The resistance curves under other currents were also measured, and h_x was then extracted and plotted in Fig. 3(b). Although both the field-like and damping-like terms of SOT can be simultaneously produced in the in-plane magnetized FM/HM bilayer, only the filed-like SOT is detected by using the PHE measurement.[23] Notice that I flows along y and H is along x in the transverse PHE configuration. The unit vector $\boldsymbol{\sigma}$ arising from SHE of top Pt layer is along x, which is parallel to the magnetization $\boldsymbol{m}$, hence the field-like SOT $\boldsymbol{m} \times \boldsymbol{\sigma} = 0$ (actually, the damping-like SOT $\boldsymbol{m} \times (\boldsymbol{\sigma} \times \boldsymbol{m}) = 0$ is also canceled).[23] This means that the effective field of field-like SOT arising from the SHE is ignorable. Hence, it seems that h_x consists only of the current-induced Oersted field h_{Oe} in the NiFe/Pt bilayer,[23] which was usually calculated by Ampere's law by assuming all current flowing through a Pt layer. It is surprising that, however, the measured h_x is far larger than the Oersted field, as shown in Fig. 3(b). This indicates that an additional effective field exists and plays a dominant role.

In addition to the SHE of Pt layer, the contribution of the interfacial Rashba SOC to field-like SOT should be considered in NiFe/Pt bilayer,[22] because the NiFe layer has two different interface structures, which are SiO_2/NiFe and NiFe/Pt. The Rashba effect appears as an effective field, which lies in the plane and transverse to the current.[29] Therefore, for NiFe/Pt bilayer, the field-like effective torque field h_{FL} should consists of the bulk spin-orbit effective field h_{FL}^{b} coming from the SHE of Pt layer and the interfacial field h_{FL}^{i} arising from the interfacial SOC. More precisely, h_y is the sum of h_{Oe}, h_{FL}^{i}, and h_{FL}^{b} at the longitudinal PHE configuration as shown in Fig. 1(a), while h_x is only equal to $h_{Oe} + h_{FL}^{i}$ at the transverse configuration as shown in Fig. 1(b), respectively.

Notice that, for NiFe/Pt bilayers, h_y has been obtained in the longitudinal PHE configuration.[26] The current-dependent h_y of NiFe/Pt(3) bilayer was then added in Fig. 3(b) for comparison. Finally, we can obtain the exact bulk contribution of the field-like SOT in NiFe/Pt(3) bilayer as $h_{FL}^{b} = h_y - h_x$, and also the interfacial one as $h_{FL}^{i} = h_x - h_{Oe}$. Both of them are plotted in Fig. 3(c).

For another NiFe/Pt bilayers with various Pt thicknesses, h_x was also obtained at the transverse configuration of PHE measurement. Then, both the effective fields h_{FL}^{b} and h_{FL}^{i} were extracted by using the above processing method and plotted in Figs. 4(a) and 4(b), respectively. It is surprising that in all samples, h_{FL}^{i} is far greater than h_{FL}^{b}. One can found that both h_{FL}^{i} and h_{FL}^{b} exhibit linear dependence on the current, and decrease with increasing the thickness of Pt layer. Also, both of them are proportional to the current density j, however, free with Pt thickness, if we assume all the current flows through Pt layer, as shown in Figs. 4(c) and 4(d), respectively. Hence, we can obtain the interfacial and bulk field-like SOT coefficients $\beta^{i} = h_{FL}^{i}/j$ and $\beta^{b} = h_{FL}^{b}/j$, respectively. They remain constant within the experimental error. Apparently, for NiFe/Pt bilayers, the interfacial contribution of field-like SOT is about 4 times larger than the bulk one.

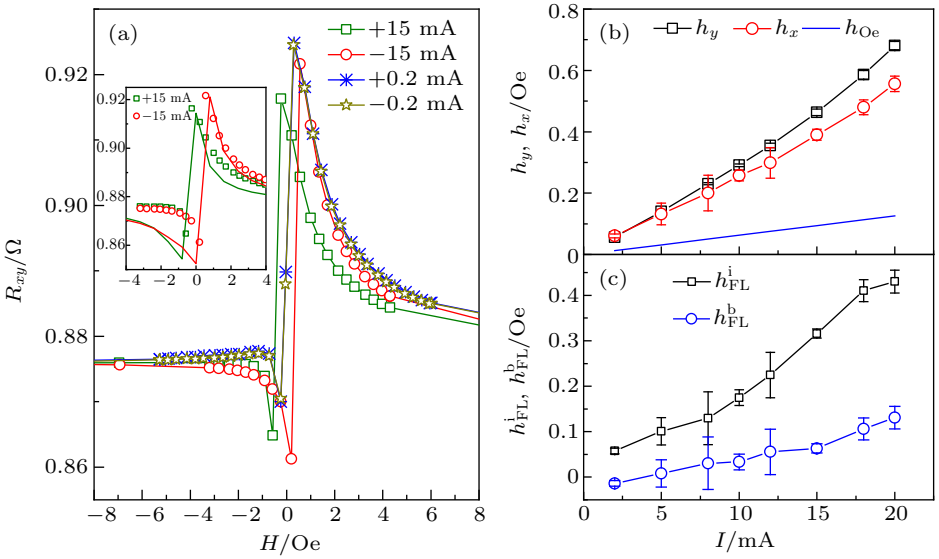


Fig. 3. The resistance and the effective field measured at the transverse PHE configuration ($I \perp H$) for NiFe(2.2)/Pt(3) bilayer. (a) The representative R_{xy}–H curves under various currents. In the inset, the solid lines are the fitting curves by using the Stoner–Wohlfarth model. (b) The current dependences of h_x and the Oersted field $h_{Oe} = I/2w$, where w is the width of the Hall bar. The field h_y was added here for comparison, which has been obtained at the longitudinal configuration.[25] (c) The current-dependent h_{FL}^{i} and h_{FL}^{b}. Here $h_{FL}^{i} = h_x - h_{Oe}$ and $h_{FL}^{b} = h_y - h_x$ are the interfacial and bulk contributions to the effective fields of current-induced field-like SOT, respectively.

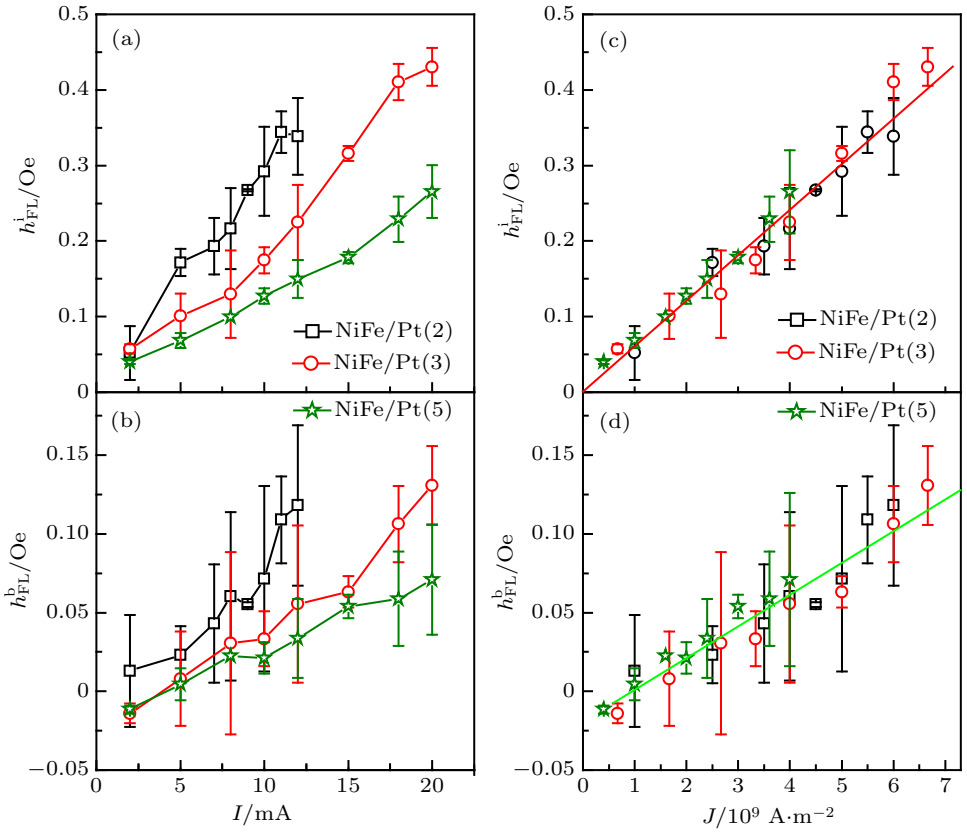


Fig. 4. Current dependences of (a) h_{FL}^{i} and (b) h_{FL}^{b} for the samples with various Pt thicknesses. The linear dependence of (c) h_{FL}^{i} and (d) h_{FL}^{b} on the current density j. All the solid lines are guides for the eyes.

In addition to the bulk field-like SOT, our results also demonstrate an interfacial field-like SOT in SiO_2/NiFe/Pt, which is similar like the finding in the Al_2O_3/NiFe/Ti.[22] The interfacial field-like SOT arises through the Rashba effect at the interface,[22] while bulk field-like SOT comes from the SHE of Pt layer.[23] Moreover, by using the PHE measurements at transverse configuration and longitudinal configuration, both the interfacial and bulk field-like SOTs have been separated in the NiFe/Pt bilayers. It is obvious that the interfacial field-like SOT is much larger than the bulk one. Our results therefore indicate that the interfacial Rashba SOC, but not the bulk SHE, dominates the current induced field-like SOT in the NiFe/Pt bilayer with asymmetric interfaces. This agrees with the previous results that, instead of the bulk SHE, the interfacial Rashba effect dominates the current induced SOT for FM/HM films with structure inversion asymmetry.[6,16,30] As was reported, via oxidizing FM layer, the interfacial SOC can be enhanced and was observed to be several times stronger than the bulk SHE.[31] Oxygen effect diffusing from the SiO_2 substrate to the NiFe layer may also occur in the sputter deposition, resulting in the enhancement of the interfacial SOC, and it may be another origin of the giant interface SOT in the SiO_2/NiFe/Pt structure. Moreover, the possible mechanism of the giant interfacial field-like SOT in NiFe/Pt bilayer may also be explained by spin-orbit precession at the interface,[32] where the polarized conduction electrons of NiFe layer are reflected from the NiFe/Pt interface and then precesses about the Rashba effective field, and in turn exert a spin torque on magnetization of NiFe layer.

5. Conclusions

The PHE method has been developed to study the origin of the current-induced SOT in a typical NiFe/Pt bilayer deposited on the SiO_2/Si substrate. It is demonstrated that both interfacial and bulk field-like SOTs in the NiFe/Pt bilayers exist. Using the PHE measurements at transverse configuration ($I \perp H$) and longitudinal configuration ($I \parallel H$), the interfacial and bulk contributions to the field-like SOT are separated. Then we can directly determine the spin-orbit effective field arising from spin Hall effect of Pt layer. Moreover, the interfacial spin-orbit effective field arising from interfacial SOC is also obtained, which is much greater than the bulk one. The giant interface SOT in NiFe/Pt bilayers suggests that further analysis of interfacial effects on the current-induced manipulation of magnetization is necessary.

References

[1] Brataas A and Hals K M D 2014 *Nat. Nanotechnol.* **9** 86
[2] Gambardella P and Miron I M 2011 *Philos. Trans. A. Math. Phys. Eng. Sci.* **369** 3175
[3] Haney P M, Lee H W, Lee K J, Manchon A and Stiles M D 2013 *Phys. Rev. B* **87** 174411
[4] Ralph D and Stiles M 2008 *J. Magn. Magn. Mater.* **320** 1190

[5] Brataas A, Tserkovnyak Y, Bauer G E W and Kelly P J 2012 *Spin Pumping and Spin Transfer in Spin Current* (Oxford: Oxford University Press) chap 8 p. 87

[6] Miron I M, Garello K, Gaudin G, Zermatten P J, Costache M V, Auffret S, Bandiera S, Rodmacq B, Schuhl A and Gambardella P 2011 *Nature* **476** 189

[7] Liu L, Pai C F, Li Y, Tseng H W, Ralph D C and Buhrman R A 2012 *Science* **336** 555

[8] Yu G, Upadhyaya P, Fan Y, Alzate J G, Jiang W, Wong K L, Takei S, Bender S A, Chang L T, Jiang Y, Lang M, Tang J, Wang Y, Tserkovnyak Y, Amiri P K and Wang K L 2014 *Nat. Nanotechnol.* **9** 548

[9] Feng X Y, Zhang Q H, Zhang H W, Zhang Y, Zhong R, Lu B W, Cao J W and Fan X L 2019 *Chin. Phys. B* **28** 107105

[10] Ramaswamy R, Lee J M, Cai K and Yang H 2018 *Appl. Phys. Rev.* **5** 031107

[11] Zhao Y C, Yang G, Dong B W, Wang S G, Wang C, Sun Y, Zhang J Y and Yu G H 2016 *Chin. Phys. B* **25** 077501

[12] Avci C O, Rosenberg E, Baumgartner M, Beran L, Quindeau A, Gambardella P, Ross C A and Beach G S D 2017 *Appl. Phys. Lett.* **111** 072406

[13] Gabor M, Petrisor T, Mos R B, Mesaros A, Nasui M, Belmeguenai M, Zighem F and Tiusan C 2016 *J. Phys. D: Appl. Phys.* **49** 365003

[14] Hsu W H, Bell R and Victora R H 2018 *IEEE Trans. Magn.* **54** 3401205

[15] Garello K, Miron I M, Avci C O, Freimuth F, Mokrousov Y, Blügel S, Auffret S, Boulle O, Gaudin G and Gambardella P 2013 *Nat. Nanotechnol.* **8** 587

[16] Miron I M, Gaudin G, Auffret S, Rodmacq B, Schuhl A, Pizzini S, Vogel J and Gambardella P 2010 *Nat. Mater.* **9** 230

[17] Haazen P P J, Muré E, Franken J H, Lavrijsen R, Swagten H J M and Koopmans B 2013 *Nat. Mater.* **12** 299

[18] Liu L Q, Lee O J, Gudmundsen T J, Ralph D C and Buhrman R A 2012 *Phys. Rev. Lett.* **109** 096602

[19] Kim J, Sinha J, Hayashi M, Yamanouchi M, Fukami S, Suzuki T, Mitani S and Ohno H 2013 *Nat. Mater.* **12** 240

[20] Zheng Z C, Guo Q X, Jo D, Go D, Wang L H, Chen H C, Yin W, Wang X M, Yu G H, He W, Lee H W, Teng J and Zhu T 2020 *Phys. Rev. Res.* **2** 013127

[21] Qiu X P, Deorani P, Narayanapillai K, Lee K S, Lee K J, Lee H W and Yang H S 2015 *Sci. Rep.* **4** 4491

[22] Emori S, Nan T X, Belkessam A M, Wang X J, Matyushov A D, Babroski C J, Gao Y, Lin H and Sun N X 2016 *Phys. Rev. B* **93** 180402(R)

[23] Fan X, Wu J, Chen Y, Jerry M J, Zhang H and Xiao J Q 2013 *Nat. Commun.* **4** 1799

[24] Zhou X, Tang M, Fan X L, Qiu X P and Zhou S M 2016 *Phys. Rev. B* **94** 144427

[25] Wang L, Wesselink R J H, Liu Y, Yuan Z, Xia K and Kelly R J 2016 *Phys. Rev. Lett.* **116** 196602

[26] Li S F and Zhu T 2020 *Jpn. J. Appl. Phys.* **59** 040906

[27] Thanh N T, Chun M G, Schmalhorst J, Reiss G, Kim K Y and Kim C G 2006 *J. Magn. Magn. Mater.* **304** e84

[28] Li G H, Yang T, Hu Q and Lai W Y 2000 *Appl. Phys. Lett.* **77** 1032

[29] Manchon A, Koo H C, Nitta J, Frolov S M and Duine R A 2015 *Nat. Mater.* **14** 871

[30] Miron I M, Moore T, Szambolics H, Buda L D, Auffret S, Rodmacq B, Pizzini S, Vogel J, Bonfim M, Schuhl A and Gaudin G 2011 *Nat. Mater.* **10** 419

[31] Qiu X P, Narayanapillai K, Wu Y, Deorani P, Yang D H, Noh W S, Park J H, Lee K J, Lee H W and Yang H 2015 *Nat. Nanotechnol.* **10** 333

[32] Greening R W, Smith D A, Lin Y M, Jiang Z J, Barber J, Dail S, Heremans J J and Emori S 2020 *Appl. Phys. Lett.* **116** 052402